Shp2 plays a crucial role in cell structural orientation and force polarity in response to matrix rigidity

Hsiao-Hui Lee[a,1], Hsin-Chang Lee[a], Chih-Chiang Chou[a], Sung Sik Hur[b,c], Katie Osterday[c,d,2], Juan C. del Álamo[c,d], Juan C. Lasheras[b,c,d], and Shu Chien[b,c,1]

[a]Department of Life Sciences and Institute of Genome Sciences, National Yang-Ming University, Taipei 11221, Taiwan, Republic of China; and [b]Department of Bioengineering, [c]Institute of Engineering in Medicine, and [d]Department of Mechanical and Aerospace Engineering, University of California at San Diego, La Jolla, CA 92093

Contributed by Shu Chien, December 28, 2012 (sent for review October 29, 2012)

Cells can sense and respond to physical properties of their surrounding extracellular matrix. We have demonstrated here that tyrosine phosphatase Shp2 plays an essential role in the response of mouse embryonic fibroblasts to matrix rigidity. On rigid surfaces, large focal adhesions (FAs) and anisotropically oriented stress fibers are formed, whereas cells plated on compliant substrates form numerous small FAs and radially oriented stress fibers. As a result, traction force is increased and organized to promote cell spreading and elongation on rigid substrates. Shp2-deficient cells do not exhibit the stiffness-dependent increase in FA size and polarized stress fibers nor the intracellular tension and cell shape change. These results indicate the involvement of Shp2 in regulating the FAs and the cytoskeleton for force maintenance and organization. The defect of FA maturation in Shp2-deficient cells was rescued by expressing Y722F Rho-associated protein kinase II (ROCKII), suggesting that ROCKII is the molecular target of Shp2 in FAs for the FA maturation. Thus, Shp2 serves as a key mediator in FAs for the regulation of structural organization and force orientation of mouse embyonic fibroblasts in determining their mechanical polarity in response to matrix rigidity.

mechanotransduction | mechanosensing | cytoskeletal architecture | phosphorylation

The interactions between adherent cells and the extracellular matrix (ECM) are essential for many cellular processes, including proliferation, differentiation, and migration (1–3). It is known that cells can sense the extracellular mechanical cues and respond to these cues by modulating cellular biochemical activities and intracellular force, a process called mechanotransduction (4–7). The altered intracellular cytoskeletal forces modulate cell shape and control complex cell behaviors that are critical for tissue development and homeostasis (8–10). Focal adhesions (FAs) link the cell to the ECM at sites of integrin binding and play dual roles in force transmission and signal transduction (11, 12). When a nascent adhesion is formed, the activated integrin links to cytoskeleton via a talin-mediated connection and requires actin-related protein-2/3 (ARP2/3) complex-mediated actin polymerization that is independent of myosin II activity (13, 14). Thereafter, some adhesions disassemble, whereas other adhesions mature through myosin-mediated contractility that promotes the recruitment of additional cytoskeletal and signaling proteins to the FAs for adhesion strengthening and signal transmission (15–19). Therefore, the FAs are mechanosensitive, and the regulation of FA dynamics plays an important role in mechanotransduction (11, 12, 20).

Abnormal cell and tissue responses to mechanical stress have been shown to contribute to the etiology and clinical presentation of many diseases or developmental disorders (21). Tyrosine phosphatase Shp2, encoded by the *PTPN11* gene, is a ubiquitously expressed, nonreceptor protein tyrosine phosphatase (PTP) (22). Germline mutations in *PTPN11* cause Noonan syndrome (gain of function) and Leopard syndrome (catalytically defective), which involve developmental abnormalities and clinical features that are strongly associated with defects in mechanotransduction (23–26). A targeting deletion of *PTPN11* exon 3 (encoding 46–110 aa) in homozygous mice led to embryonic death during gastrulation with severe defects in mesodermal patterning (27, 28), indicating the functional deficiency of Shp2 caused by exon 3 deletion. No phenotype was found in heterozygous mice. In addition, mouse embryonic fibroblasts (MEFs) derived from the $Shp2^{Ex3-/-}$ embryos displayed severe defects in cell migration, which could be rescued by the reintroduction of wild-type Shp2 (29).

The spatiotemporal control of small GTPase RhoA/Rho-associated protein kinase (ROCK)-mediated actomyosin contractility plays a key role in regulating FA dynamics. A reduction in contractility leads to FA disassembly, and enhanced contractility causes FA stabilization and maturation; these changes affect the cellular response to extracellular stimuli such as matrix rigidity. Importantly, RhoA/ROCK signaling is involved in the regulation of stem cell lineage commitment by mechanical forces, emphasizing the importance of RhoA/ROCK signaling in mechanotransduction (2, 30, 31). Our previous studies showed that the RhoA-mediated ROCKII activation is negatively regulated by ROCKII phosphorylation at Y722 residue. Protein kinase Src and Shp2 phosphatase reciprocally modulate this regulation specifically at FAs (32, 33). In this report, we demonstrated that Shp2 plays a key role in the maturation of FAs and the regulation of stress-fiber orientation during the cellular response to matrix rigidity. By traction force microscopy (TFM), we found that $Shp2^{Ex3-/-}$ cells bear lower intracellular tension than wild-type cells ($Shp2^{WT}$), confirming the involvement of Shp2 in regulating the FAs and the cytoskeleton for force maintenance and organization. Moreover, we demonstrated the recruitment of Shp2 in FAs and its correlation with the decrease of ROCKII Y722 phosphorylation in FAs. By rescuing FA maturation via expression of Y722F ROCKII in $Shp2^{Ex3-/-}$ cells, we also provide evidence that ROCKII is the molecular target of Shp2 in FAs. In summary, our study provides new insight into the role of Shp2 in mechanotransduction by showing that, when cells respond to the increase of matrix rigidity, Shp2 participates in FAs to promote their maturation through ROCKII Y722 dephosphorylation, which in turn contributes to stress-fiber polarization and enhanced intracellular tension.

Results

Shp2 Is Required for Matrix-Stiffness–Mediated FA Maturation and Stress-Fiber Polarization. FAs anchor cells to the ECM, serving as mechanosensors and providing mechanical support for stress fibers that bear the intracellular tension (11, 12). To test whether Shp2 is involved in the cellular response to matrix rigidity, $Shp2^{WT}$

Author contributions: H.-H.L., J.C.d.Á., J.C.L., and S.C. designed research; H.-H.L., H.-C.L., and C.-C.C. performed research; S.S.H., K.O., and J.C.d.Á. contributed new reagents/analytic tools; H.-H.L., H.-C.L., S.S.H., K.O., and J.C.d.Á. analyzed data; and H.-H.L., J.C.d.Á., and S.C. wrote the paper.

The authors declare no conflict of interest.

[1]To whom correspondence may be addressed. E-mail: shuchien@ucsd.ed or hhl@ym.edu.tw.

[2]Deceased December 20, 2012.

This article contains supporting information online at www.pnas.org/lookup/suppl/doi:10.1073/pnas.1222164110/-/DCSupplemental.

and Shp2$^{Ex3-/-}$ MEFs were plated on fibronectin (FN)-conjugated elastomeric polyacrylamide (PAA) gels with Young's modulus E = 2.5, 9.0 and 21.5 kPa, as well as on glass for 4 h. We had checked that a steady state of cell spreading of both cells was attained after a 4-h adhesion in each condition. Analysis of immunofluorescence staining of paxillin (Fig. 1*A*) showed that the size distribution of FAs in Shp2^{WT} cells varied with the substrate rigidity (Fig. 1*B*). On the softest gel (2.5 kPa), most FA areas were smaller than 0.5 μm^2. An increase of rigidity induced the formation of larger FAs (>2 μm^2), with a concomitant decrease in small FAs (Fig. 1*B*). However, as shown in Fig. 1*C*, Shp2$^{Ex3-/-}$ cells exhibited numerous small FAs regardless of matrix rigidity (9.0 and 21.5 kPa and glass); no FAs were detectable in the cells seeded on the softest gel (2.5 kPa), as these cells were not spreading. These results suggest that the modulation of FA maturation and clustering in MEFs by matrix stiffness require Shp2 function.

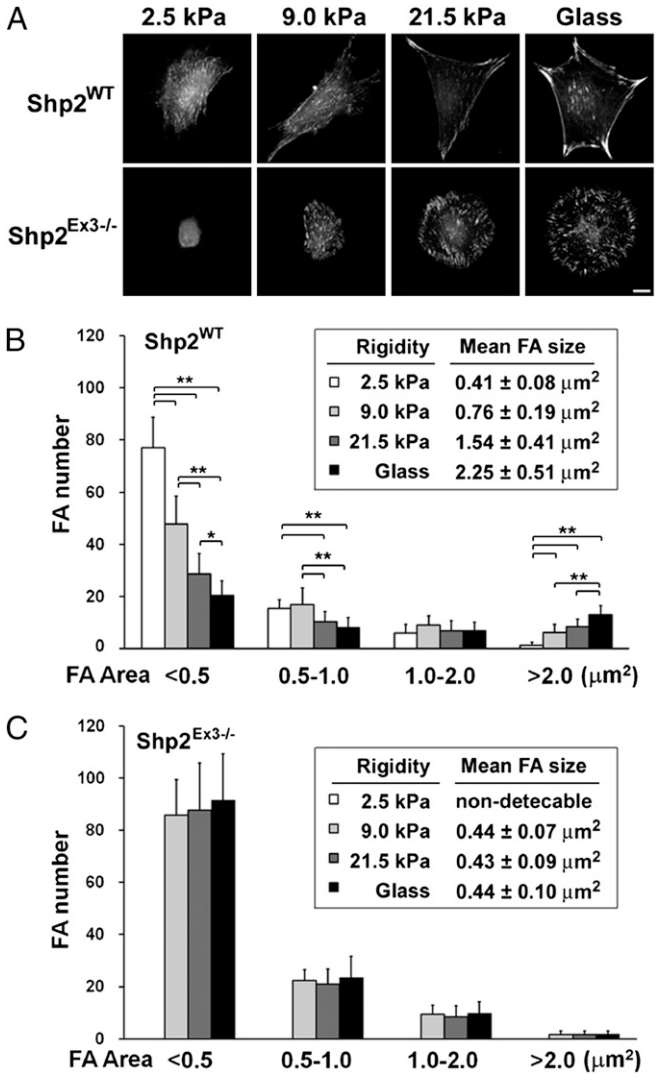

Fig. 1. Shp2 is required for matrix stiffness-dependent FA maturation in fibroblasts. (*A*) Shp2^{WT} and Shp2$^{Ex3-/-}$ MEFs seeded on PAA gel with a Young's modulus of 2.5, 9.0, or 21.5 kPa, or on glass coverslips, coated with fibronectin for 4 h, were stained with anti-paxillin antibody for FA determination. All FAs in the field were subjected to ImageJ analysis for FA quantification. (Scale bar, 10 μm.) (*B* and *C*) Numbers of FAs per cell in different sizes (areas; in micrometers squared) of Shp2^{WT} (*B*) and Shp2$^{Ex3-/-}$ (*C*) MEFs seeded on gels with different rigidities or on glass coverslips. *Inset* shows the mean FA area in each condition. All data are expressed as mean ± SD from 20 representative cells. *P < 0.005; **P < 0.0005.

It has been shown that the alignment of FAs and/or orientation of stress fibers precede cell elongation in response to matrix rigidity (34–36). To calculate the orientation of stress fibers, we analyzed the images of FITC-phalloidin stained cells using a method similar to that described by Karlon et al. (37). In order to combine the data from individual cells on a common coordinate system, each cell image is rotated so that the median stress-fiber orientation coincides with the horizontal axis (0°). Stress-fiber orientation angles between −90° and 90° are then measured counterclockwise with respect to this horizontal axis. A map displaying the local orientation of the stress fibers with respect to the median stress-fiber orientation is shown in Fig. 2*A*. The polar histograms of stress-fiber orientations are shown in Fig. 2*B*. The spread of the distribution of stress-fiber orientations, as indicated by the standard deviation, provides a measure of the degree of stress-fiber polarization. Fig. 2*B* shows that the Shp2^{WT} cells seeded on the more rigid matrices had higher degrees of alignment of stress-fiber orientations. Shp2$^{Ex3-/-}$ cells exhibited wider distributions of stress-fiber orientation than Shp2^{WT} cells and showed little change as the matrix rigidity was increased. These findings suggest that Shp2 plays an important role in the stiffness-dependent FA maturation and anisotropic orientation of stress fibers in MEFs.

Shp2 Deficiency Affects Cell Shape and Intracellular Tension. The spreading of a cell involves shape changes that produce mechanical stresses inside the cell and in the matrix (35, 36). To further elucidate the role of Shp2 in the cellular response to matrix rigidity, we measured cell spreading shape and traction forces of Shp2^{WT} and Shp2$^{Ex3-/-}$ cells seeded on substrates with different rigidities. Fig. 3*A* shows typical examples of traction stress vector plots (T_{xy}), maps of traction stress magnitude (T_{mag}), and DIC cell images. The arrowheads indicate the stress direction, and both the width and length of the arrow stem indicate the stress magnitude (Fig. 3*A*, *Top* row). The high NA (60×) used in our DIC microscopy includes the thin ruffles of the lamellipodia, which may not be seen with a lower NA.

With an increase in matrix rigidity, Shp2^{WT} cells spread out and became more elongated. Accordingly, the cell spreading area (Fig. 3*B*), aspect ratio (Fig. 3*C*), and shape factor (ratio of the perimeter of the cell to that of a circle with an equal area, Fig. 3*D*) increased with matrix rigidity in Shp2^{WT} cells. These parameters were significantly lower in Shp2$^{Ex3-/-}$ cells. While the spreading area of Shp2$^{Ex3-/-}$ cells also increased with matrix rigidity, the cell aspect ratio and shape factor remained very low and did not vary with the level of matrix rigidity (Fig. 3 *C* and *D*), consistent with the decrease of stress-fiber polarization in these Shp2$^{Ex3-/-}$ cells.

Analysis of the traction stress measurements revealed that the net contractile moment, which is a coordinate-invariant scalar often used to infer cellular contractile strength (38), was significantly lower in Shp2$^{Ex3-/-}$ cells than in Shp2^{WT} cells (Fig. 3*E*). The traction stress measurements were processed as described by Hur et al. (39) to determine maps of intracellular tension. Tension (T) is defined as force per unit length; thus, the total force supported by the cytoskeleton at a given intracellular section is equal to the product of the intracellular tension and the length of that section (Fig. S1 and Eq. **S1**). At each location, we determined the intracellular tensions parallel to the long and short axes of the cell, T_L and T_S, respectively. While T_L was significantly lower in Shp2$^{Ex3-/-}$ cells than in Shp2^{WT} cells, T_S did not show statistically significant differences between the two types of cells (Fig. 3 *F* and *G*). This may suggest a minimum fiber length from which Sph2 function becomes activated and/or significantly important.

Whereas the loss of Shp2 function led to lower levels of cell spreading area (Fig. 3*B*), net contractile moments (Fig. 3*E*), and intracellular tension T_L (Fig. 3*F*) at all levels of rigidity, these parameters still showed a dependence on matrix rigidity in

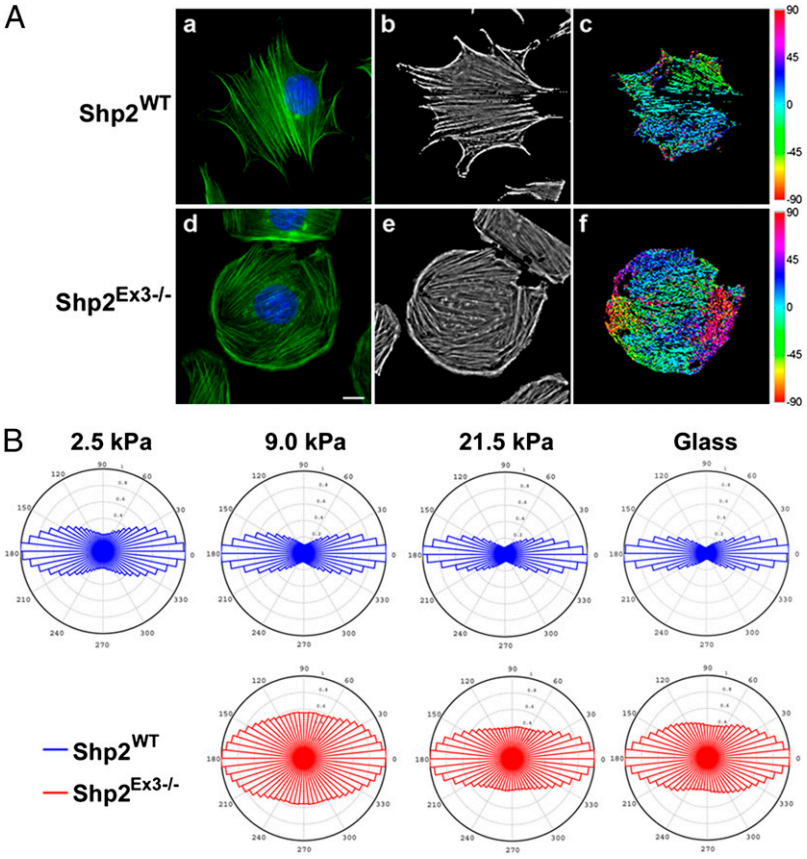

Fig. 2. Shp2 is involved in the organization of stress-fiber orientation in response to matrix rigidity. (*A*) Images of $Shp2^{WT}$ (*a*–*c*) and $Shp2^{Ex3-/-}$ (*d*–*f*) MEFs seeded on FN-coated glass. Cells were stained with FITC-phalloidin (green) for F-actin, and Hoechst (blue) for nuclei (*a* and *d*). After image segmentation, the orientation of each fiber was determined, and the image was rotated so that the median stress-fiber orientation is horizontal (*b* and *e*). Different orientations of actin filaments are depicted with different colors (*c* and *f*). (Scale bar in *d*, 10 μm.) (*B*) Histograms of stress-fiber orientations summarized from 15 $Shp2^{WT}$ (blue) and 15 $Shp2^{Ex3-/-}$ (red) cells for each level of matrix rigidity for 4 h as indicated.

$Shp2^{Ex3-/-}$ cells. Therefore, our data indicate that, although Shp2 plays an important role in the regulation of both cell shape and the directional organization of intracellular tension, the variations of these parameters with matrix rigidity still remain in $Shp2^{Ex3-/-}$ cells, albeit with significant attenuations. These results indicate that Shp2 is not a major factor for rigidity sensing.

Expression of ROCKII Y722F Rescues FA Maturation in Shp2-Deficient Cells. We have previously demonstrated that Shp2 is involved in RhoA-dependent ROCKII activation (32). To address whether Shp2 is recruited into FAs to decrease ROCKII Y722 phosphorylation, we isolated the FA fraction from $Shp2^{WT}$ and $Shp2^{Ex3-/-}$ cells using a method as described by Kuo et al (40). The cells were hypotonically shocked and then the cell bodies were removed by pulsed flow with PBS. The FA fraction was collected to examine the levels of Shp2 protein and ROCKII Y722 phosphorylation by Western blot analysis. We found that full-length Shp2 protein was clearly detected in the FA fraction isolated from $Shp2^{WT}$ cells (Fig. S2*A*). In $Shp2^{Ex3-/-}$ cells, the total protein level of exon3-deleted Shp2 was significantly lower than full-length Shp2 in $Shp2^{WT}$ cells (Fig. S2*A*); this is consistent with other reports (29, 41). Importantly, almost no mutant Shp2 protein was detected in FA fraction isolated form $Shp2^{Ex3-/-}$ cells. This finding suggests the requirement of the Shp2 domain encoded by exon3 for its FA targeting and may also explain the functional deficiency caused by the deletion of exon3 in Shp2. The FA-targeting of Shp2 was further confirmed by immunofluorescence staining of the FAs from cells after hypotonic treatment (Fig. S2*B*). The ROCKII protein was detected in the FA fraction of both types of cells. The level of ROCKII Y722 phosphorylation normalized by dividing it by the ROCKII protein level of the same sample was significantly higher in $Shp2^{Ex3-/-}$ cells than $Shp2^{WT}$ cells (Fig. S2*A*). Quantification of the ratio of fluorescence densities of pY722-ROCKII to paxillin in FAs at 4 h showed that the relative level of ROCKII Y722 phosphorylation decreased in $Shp2^{WT}$ cells in response to the increase of matrix rigidity (Fig. S3). It is recognized that this ratio could vary with the stages of FA maturation. In contrast, the ROCKII Y722 phosphorylation of $Shp2^{Ex3-/-}$ cells at all matrix rigidities (9.0 kPa, 21.5 kPa, and glass) was at a level higher than those seen in $Shp2^{WT}$ cells and was insensitive to variations in matrix rigidity. Overall, these data indicate that Shp2 participates in FAs and plays a significant role in ROCKII Y722 dephosphorylation in cellular response to matrix rigidity.

To test whether ROCKII is the molecular target of Shp2 for FA maturation, we expressed the wild type (WT) and Y722F mutant of GFP-ROCKII in $Shp2^{WT}$ and $Shp2^{Ex3-/-}$ cells and determined their FA sizes by visualizing their coexpression with RFP-vinculin (Fig. 4*A*). Y722F GFP-ROCKII expression induced a decrease in the number of small FAs (<0.5 μm^2) in both $Shp2^{WT}$ and $Shp2^{Ex3-/-}$ MEFs, compared with the corresponding cells expressing WT GFP-ROCKII. Importantly, the number of matured FAs (>2 μm^2) in $Shp2^{Ex3-/-}$ cells was markedly increased by the expression of Y722F GFP-ROCKII (Fig. 4*B*) to reach the level observed in $Shp2^{WT}$ cells. The cell shape factor of $Shp2^{Ex3-/-}$ cells was also partially restored by Y722F GFP-ROCKII (Fig. 4*C*). These results indicate that expression of Y722F ROCKII

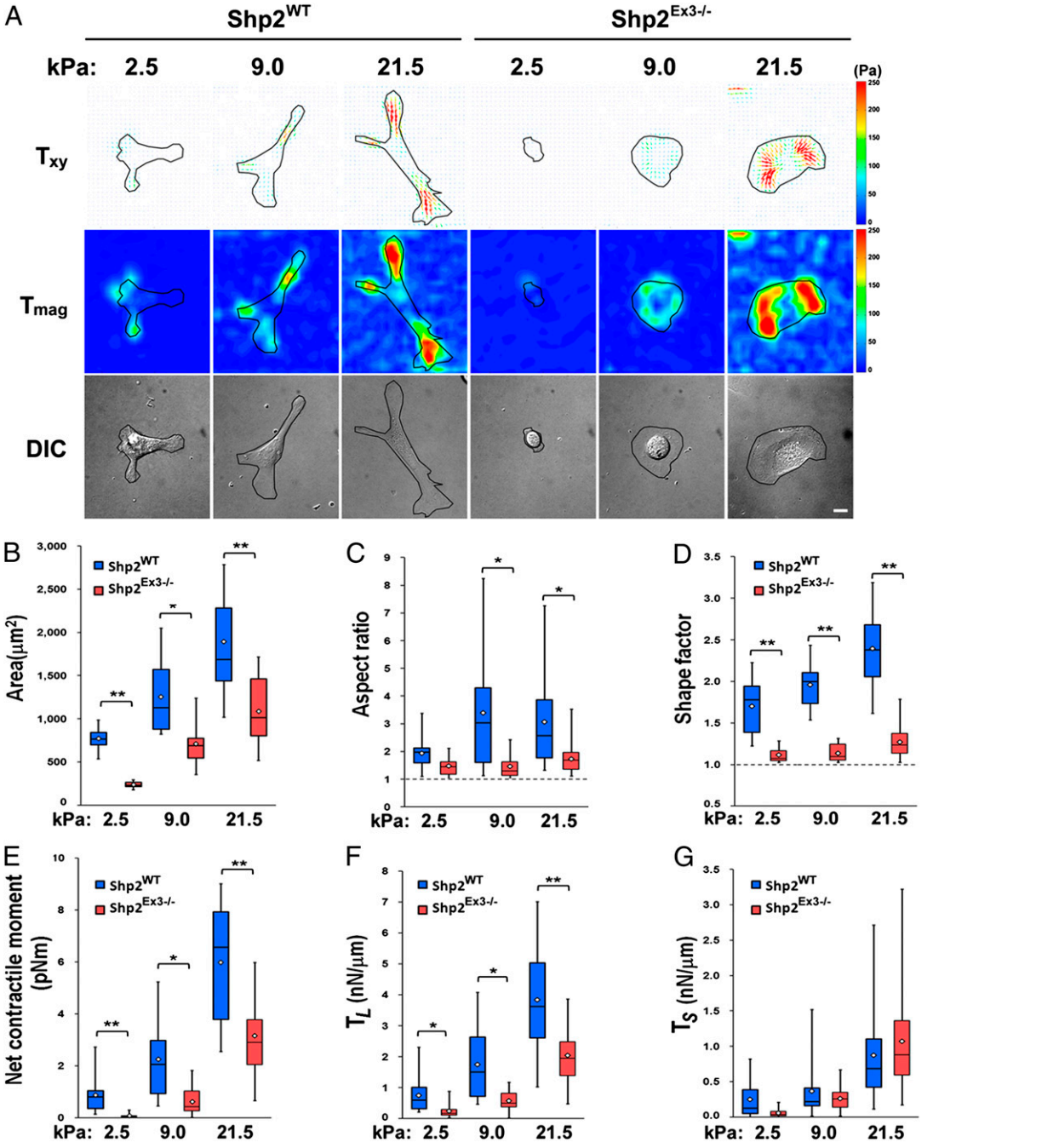

Fig. 3. Cellular traction force analysis of Shp2^{WT} and Shp2$^{Ex3-/-}$ MEFs in response to matrix rigidity. Cells were seeded on the FN-coated PAA gel with rigidities of 2.5, 9.0, or 21.5 kPa overnight. Traction fields were computed from the displacement of images of fluorescence beads, before and following cell removal by trypsin treatment. (*A*) Showing a set of representative images of traction stress vector plots (T_{xy}), maps of traction stress magnitude (T_{mag}), and DIC cell images. Arrows in T_{xy} plots show the direction of the displacement field of the traction. Colors in T_{xy} and T_{mag} maps show the magnitude of the traction vectors in the Pascal unit. (Scale bar in DIC, 10 μm.) (*B*–*G*) Box and whisker diagrams showing (*B*) cell spreading area, (*C*) aspect ratio, (*D*) shape factor, (*E*) net contractile moment, (*F*) intracellular tensions parallel to the long axes (T_L), and (*G*) intracellular tensions parallel to the short axes (T_S) of the Shp2^{WT} (blue) and Shp2$^{Ex3-/-}$ (red) MEFs. The sample numbers are 14, 12, and 20 for Shp2^{WT} and 15, 13, and 24 for Shp2$^{Ex3-/-}$ cells on the 2.5, 9.0, and 21.5 kPa gels, respectively. *$P < 0.005$; **$P < 0.0005$.

was able to rescue the defect of FA maturation in Shp2$^{Ex3-/-}$ cells, thus further establishing the role of ROCKII (Y722) in FA maturation.

Discussion

The rigidity of the ECM influences many cellular processes, including cell adhesion, migration, growth, differentiation, and gene expression (2, 42, 43). In this study, we used MEFs to address the role of Shp2 in their response to ECM rigidity. Comparison of the results on Shp2^{WT} and Shp2$^{Ex3-/-}$ MEFs showed that Shp2 is required for the maturation of FAs and the anisotropic orientation of stress fibers in response to matrix rigidity. Concurrently, the loss of Shp2 function in the FAs leads to marked reductions in both the alignment of stress-fiber orientation and net contractile

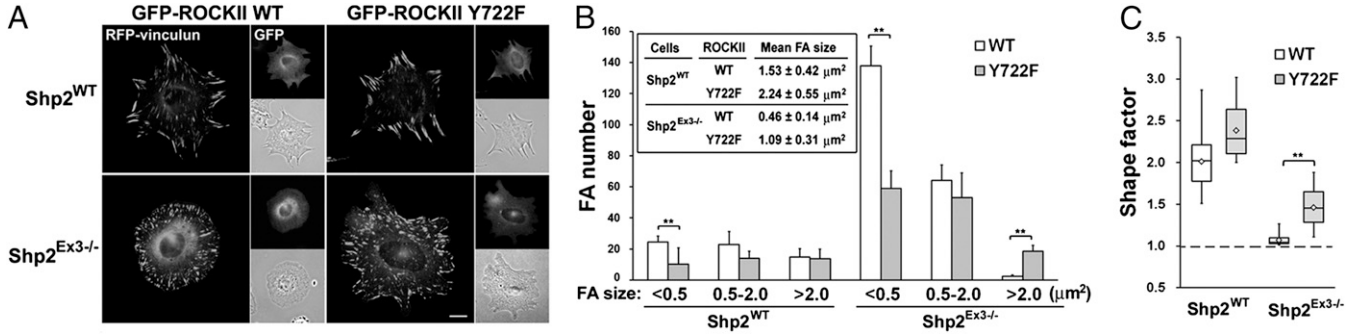

Fig. 4. Expression of ROCKII Y722F rescues FA maturation in $Shp2^{Ex3-/-}$ MEFs. (*A*) $Shp2^{WT}$ and $Shp2^{Ex3-/-}$ MEFs were cotransfected with pRFP-vinculin and pGFP-ROCKII WT or Y722F for 24 h, and then replated onto FN-coated coverslips for 2 h. (Scale bar, 10 μm.) (*B*) Number of FAs per cell in different sizes (area; in micrometers squared) under different conditions are shown. *Inset* shows the mean FA area in each condition ($n = 10$). (*C*) Cellular shape factors are shown ($n = 20$). $*P < 0.005$; $**P < 0.0005$.

moment inside the cell, thus blunting the cell polarization in response to the increase of matrix rigidity. Furthermore, the responses of MEFs to ECM rigidity involve the participation of Shp2 in FAs, where it contributes to the reduction of ROCKII Y722 phosphorylation. The defect of FA maturation in $Shp2^{Ex3-/-}$ cells was rescued by expressing unphosphorylable GFP-ROCKII Y722F, suggesting that ROCKII is the molecular target of Shp2 in FAs for the stiffness-dependent FA maturation in MEFs. These results indicate that Shp2 plays a key role in mechanotransduction in response to increased ECM rigidity by decreasing ROCKII Y722 phosphorylation in FAs to enhance FA maturation and facilitate the directional orientation of stress fibers and the spatial organization of intracellular forces.

ECM rigidity can be sensed by the force-sensing molecules that are mechanically linked to ECM-ligand integrins and actin filaments, thus resulting in cell deformation by changes in the mechanical forces transmitted between the ECM and the cytoskeleton (43, 44). These changes may allow the signaling molecules to bind the force-sensing molecules to elicit the biochemical signals involved in the cellular responses to the matrix rigidity (45). $Shp2^{Ex3-/-}$ cells, as $Shp2^{WT}$ cells, can increase their spreading area and intracellular tension (T_L) in response to an increase in Young's modulus of the ECM, indicating that $Shp2^{Ex3-/-}$ cells are still able to sense ECM rigidity, though in an attenuated manner. When cells sense the rigid matrix, the FAs grow and recruit proteins to enhance contraction force that leads to the rearrangement of FAs and orientation of stress fibers. These changes cause the spatial organization of intracellular forces and hence changes in cell shape and a reinforcement of cellular tension. Therefore, the significantly lower stiffness-dependent changes of FA size, stress-fiber polarization, cell shape, and direction of intracellular tension in $Shp2^{Ex3-/-}$ cells indicate that the loss of Shp2 function in FAs leads to a defective response to ECM rigidity.

Rigidity response is a case of mechanotransduction in which the variations in ECM compliance are converted into intracellular biochemical signals such as protein activities. It is well known that the differential tyrosine phosphorylations of adhesion molecules and their associated proteins play key roles in regulating FA dynamics (44, 46–48). Prager-Khoutorsky et al. recently showed the roles of different protein tyrosine kinases (PTKs) in the ECM stiffness-dependent fibroblast polarization (34). They delineated the mechanosensitive cell polarization into several stages, beginning with the radial spreading of the cell attached to ECM and followed by the formation of dot-like nascent FAs in its periphery. Owing to the development of mechanical forces at the nascent FAs, these adhesions grow and rearrange their distribution and direction to establish the cell polarization axis. The FAs oriented parallel to the major axis of the cell keep growing and elongating, whereas the FAs oriented in other directions become disassembled. As a result, cells become fully polarized with matured FAs at their leading and trailing edges. Multiple PTKs were found to be involved in the regulation of these stages (34). In our study, we found that Shp2 is involved in the rigidity response by dephosphorylating ROCKII Y722 in FAs to facilitate FA maturation and cause the rearrangement of stress fibers and the directional organization of the intracellular forces. Interestingly, we found that $Shp2^{Ex3-/-}$ cells have a phenotype similar to one group of PTK knockdowns (protein tyrosine kinases CSK1R, CSK, FER, ERBB4, and FLT3) (34). In particular, CSK serves as an inhibitor of Src kinase, which is responsible for ROCKII Y722 phosphorylation in FAs. CSK-knockdown cells exhibited immature FAs, low tension force, and decreased cell elongation on both rigid and compliant surfaces (34), similar to the $Shp2^{Ex3-/-}$ cells.

Different studies suggest that Shp2 can either positively (49–51) or negatively (52, 53) regulate RhoA activity. Thus, Shp2 can decrease RhoA activity by inhibiting guanine nucleotide exchange factor Vav2 (53), whereas it can also increase RhoA activity by inhibiting Rho family GTPase-activating protein p190RhoGAP (49, 50). In addition, Shp2 can also promote Src activation directly by dephosphorylating the inhibitory phosphotyrosine on the Src C terminus and indirectly by decreasing Csk recruitment, that activates p190RhoGAP and results in RhoA suppression (54). Under our experimental condition, GST-Rho-binding domain (RBD) pull-down assays showed similar RhoA activities in $Shp2^{WT}$ and $Shp2^{Ex3-/-}$ MEFs seeded on soft and rigid gels (Fig. S4). However, the ROCKII activation, as indicated by S1366 phosphorylation (55), increased in response to increasing ECM rigidity in $Shp2^{WT}$ cells, but not in $Shp2^{Ex3-/-}$ cells (Fig. S5); this finding is consistent with the stiffness-dependent reduction of ROCKII Y722 phosphorylation in wild-type cells (Fig. S3). Furthermore, expression of catalytic-dead Shp2 (C/S) mutant in NIH3T3 stable line expressing wild-type ROCKII significantly reduced the size of FAs, whereas this manipulation had no effect on NIH3T3 stable line expressing Y722F ROCKII (Fig. S6). Overall, these data suggest that ROCKII is the molecular target of Shp2 in FAs for the stiffness-dependent FA maturation.

Von Wichert et al. demonstrated that Shp2 is required for the formation of force-dependent integrin-cytoskeleton linkages (56). Here, we show that the deficiency of Shp2 leads to decreases in net contractile moments and intracellular tension (T_L) in comparison to WT cells at the same level of ECM rigidity (Fig. 3 *E* and *F*). In particular, we demonstrated that the directional organization of the cytoskeleton and the intracellular tension were significantly reduced in the Shp2 mutants. Based on these results, we conclude that, in addition to contributing to FA maturation and the strengthening of mechanical forces at the

FAs, Shp2 regulates the spatiotemporal dynamics of FAs and contributes to the directional rearrangement of stress fibers and force organization, thus playing an important role in determining the mechanical polarity in cellular response to matrix rigidity.

Materials and Methods

The experimental materials and methods are described in brief here; detailed information is provided in *SI Materials and Methods*. $Shp2^{WT}$ and $Shp2^{Ex3-/-}$ MEFs were kindly provided by Gen-Sheng Feng (Molecular Pathology Graduate Program, University of California, San Diego) (29). PAA gels were prepared based on the method developed by Wang and colleagues (57). The final concentration of acrylamide/Bis-acrylamide was 5%/0.1%, 10%/0.1%, and 10%/0.2% (vol/vol) for 2.5, 9.0, and 21.5 kPa gels, respectively. The substrate deformation field was obtained from the lateral displacements of fluorescent beads embedded in the gel. The lateral traction stresses exerted by the cells were determined from the measured substrate deformation after solving the equation of static equilibrium for an elastic substrate, as described previously (58). The net contractile moment (M) was calculated from the measured traction stresses as described in *SI Materials and Methods* (and refs. 34, 38). The intracellular tension along the major (T_L) and minor (T_S) axes were determined as described by Hur et al. (39).

ACKNOWLEDGMENTS. We thank Dr. Gen-Sheng Feng [Department of Pathology, School of Medicine, University of California, San Diego (UCSD)] for the $Shp2^{WT}$ and $Shp2^{Ex3-/-}$ MEFs. This research is supported by Taiwan National Science Council (NSC100-2320-B-010-021 and NSC101-2320-B-010-070), and in part by the University System of Taiwan–UCSD International Research-Intensive Center of Excellence (I-RiCE) in Advanced Bioengineering sponsored by the Taiwan National Science Council Program (NSC-101-2911-I-009-101), National Institutes of Health Research Grants 1R01GM084227 (to J.C.L.) and 1R01HL108735 (to S.C.), National Science Foundation NANC740 (to S.C.), and California Institute of Regenerative Medicine Grant RT-2-01889 (to S.C.).

1. Mammoto A, Ingber DE (2009) Cytoskeletal control of growth and cell fate switching. *Curr Opin Cell Biol* 21(6):864–870.
2. Engler AJ, Sen S, Sweeney HL, Discher DE (2006) Matrix elasticity directs stem cell lineage specification. *Cell* 126(4):677–689.
3. Levental KR, et al. (2009) Matrix crosslinking forces tumor progression by enhancing integrin signaling. *Cell* 139(5):891–906.
4. Discher DE, Janmey P, Wang YL (2005) Tissue cells feel and respond to the stiffness of their substrate. *Science* 310(5751):1139–1143.
5. Wang N, Tytell JD, Ingber DE (2009) Mechanotransduction at a distance: Mechanically coupling the extracellular matrix with the nucleus. *Nat Rev Mol Cell Biol* 10(1):75–82.
6. Jaalouk DE, Lammerding J (2009) Mechanotransduction gone awry. *Nat Rev Mol Cell Biol* 10(1):63–73.
7. Ingber DE (1997) Integrins, tensegrity, and mechanotransduction. *Gravit Space Biol Bull* 10(2):49–55.
8. Chowdhury F, et al. (2010) Material properties of the cell dictate stress-induced spreading and differentiation in embryonic stem cells. *Nat Mater* 9(1):82–88.
9. Wozniak MA, Chen CS (2009) Mechanotransduction in development: A growing role for contractility. *Nat Rev Mol Cell Biol* 10(1):34–43.
10. Kolahi KS, Mofrad MR (2010) Mechanotransduction: A major regulator of homeostasis and development. *Wiley Interdiscip Rev Syst Biol Med* 2(6):625–639.
11. Schwartz MA, DeSimone DW (2008) Cell adhesion receptors in mechanotransduction. *Curr Opin Cell Biol* 20(5):551–556.
12. Geiger B, Spatz JP, Bershadsky AD (2009) Environmental sensing through focal adhesions. *Nat Rev Mol Cell Biol* 10(1):21–33.
13. Harburger DS, Calderwood DA (2009) Integrin signalling at a glance. *J Cell Sci* 122(Pt 2):159–163.
14. Zhang X, et al. (2008) Talin depletion reveals independence of initial cell spreading from integrin activation and traction. *Nat Cell Biol* 10(9):1062–1068.
15. del Rio A, et al. (2009) Stretching single talin rod molecules activates vinculin binding. *Science* 323(5914):638–641.
16. Parsons JT, Horwitz AR, Schwartz MA (2010) Cell adhesion: Integrating cytoskeletal dynamics and cellular tension. *Nat Rev Mol Cell Biol* 11(9):633–643.
17. Webb DJ, Parsons JT, Horwitz AF (2002) Adhesion assembly, disassembly and turnover in migrating cells—over and over and over again. *Nat Cell Biol* 4(4):E97–E100.
18. Huveneers S, Danen EH (2009) Adhesion signaling: Crosstalk between integrins, Src and Rho. *J Cell Sci* 122(Pt 8):1059–1069.
19. Zaidel-Bar R, Itzkovitz S, Ma'ayan A, Iyengar R, Geiger B (2007) Functional atlas of the integrin adhesome. *Nat Cell Biol* 9(8):858–867.
20. Kaazempur Mofrad MR, et al. (2005) Exploring the molecular basis for mechanosensation, signal transduction, and cytoskeletal remodeling. *Acta Biomater* 1(3):281–293.
21. Ingber DE (2003) Mechanobiology and diseases of mechanotransduction. *Ann Med* 35(8):564–577.
22. Neel BG, Gu H, Pao L (2003) The 'Shp'ing news: SH2 domain-containing tyrosine phosphatases in cell signaling. *Trends Biochem Sci* 28(6):284–293.
23. Grossmann KS, Rosário M, Birchmeier C, Birchmeier W (2010) The tyrosine phosphatase Shp2 in development and cancer. *Adv Cancer Res* 106:53–89.
24. Chan G, Kalaitzidis D, Neel BG (2008) The tyrosine phosphatase Shp2 (PTPN11) in cancer. *Cancer Metastasis Rev* 27(2):179–192.
25. Kontaridis MI, Swanson KD, David FS, Barford D, Neel BG (2006) PTPN11 (Shp2) mutations in LEOPARD syndrome have dominant negative, not activating, effects. *J Biol Chem* 281(10):6785–6792.
26. Ogata T, Yoshida R (2005) PTPN11 mutations and genotype-phenotype correlations in Noonan and LEOPARD syndromes. *Pediatr Endocrinol Rev* 2(4):669–674.
27. Saxton TM, Pawson T (1999) Morphogenetic movements at gastrulation require the SH2 tyrosine phosphatase Shp2. *Proc Natl Acad Sci USA* 96(7):3790–3795.
28. Saxton TM, et al. (1997) Abnormal mesoderm patterning in mouse embryos mutant for the SH2 tyrosine phosphatase Shp-2. *EMBO J* 16(9):2352–2364.
29. Yu DH, Qu CK, Henegariu O, Lu X, Feng GS (1998) Protein-tyrosine phosphatase Shp-2 regulates cell spreading, migration, and focal adhesion. *J Biol Chem* 273(33):21125–21131.
30. McBeath R, Pirone DM, Nelson CM, Bhadriraju K, Chen CS (2004) Cell shape, cytoskeletal tension, and RhoA regulate stem cell lineage commitment. *Dev Cell* 6(4):483–495.
31. Connelly JT, et al. (2010) Actin and serum response factor transduce physical cues from the microenvironment to regulate epidermal stem cell fate decisions. *Nat Cell Biol* 12(7):711–718.
32. Lee HH, Chang ZF (2008) Regulation of RhoA-dependent ROCKII activation by Shp2. *J Cell Biol* 181(6):999–1012.
33. Lee HH, et al. (2010) Src-dependent phosphorylation of ROCK participates in regulation of focal adhesion dynamics. *J Cell Sci* 123(Pt 19):3368–3377.
34. Prager-Khoutorsky M, et al. (2011) Fibroblast polarization is a matrix-rigidity-dependent process controlled by focal adhesion mechanosensing. *Nat Cell Biol* 13(12):1457–1465.
35. Zemel A, Rehfeldt F, Brown AE, Discher DE, Safran SA (2010) Optimal matrix rigidity for stress fiber polarization in stem cells. *Nat Phys* 6(6):468–473.
36. Zemel A, Rehfeldt F, Brown AE, Discher DE, Safran SA (2010) Cell shape, spreading symmetry and the polarization of stress-fibers in cells. *J Phys Condens Matter* 22(19):194110.
37. Karlon WJ, et al. (1999) Measurement of orientation and distribution of cellular alignment and cytoskeletal organization. *Ann Biomed Eng* 27(6):712–720.
38. Butler JP, Tolić-Nųrrelykke IM, Fabry B, Fredberg JJ (2002) Traction fields, moments, and strain energy that cells exert on their surroundings. *Am J Physiol Cell Physiol* 282(3):C595–C605.
39. Hur SS, et al. (2012) Roles of cell confluency and fluid shear in 3-dimensional intracellular forces in endothelial cells. *Proc Natl Acad Sci USA* 109(28):11110–11115.
40. Kuo JC, Han X, Hsiao CT, Yates JR, 3rd, Waterman CM (2011) Analysis of the myosin-II-responsive focal adhesion proteome reveals a role for β-Pix in negative regulation of focal adhesion maturation. *Nat Cell Biol* 13(4):383–393.
41. Qu CK, et al. (1997) A deletion mutation in the SH2-N domain of Shp-2 severely suppresses hematopoietic cell development. *Mol Cell Biol* 17(9):5499–5507.
42. Lo CM, Wang HB, Dembo M, Wang YL (2000) Cell movement is guided by the rigidity of the substrate. *Biophys J* 79(1):144–152.
43. Vogel V, Sheetz M (2006) Local force and geometry sensing regulate cell functions. *Nat Rev Mol Cell Biol* 7(4):265–275.
44. Giannone G, Sheetz MP (2006) Substrate rigidity and force define form through tyrosine phosphatase and kinase pathways. *Trends Cell Biol* 16(4):213–223.
45. Bao G, et al. (2010) Molecular biomechanics: The molecular basis of how forces regulate cellular function. *Mol Cell Biomech* 3(2):91–105.
46. Mitra SK, Hanson DA, Schlaepfer DD (2005) Focal adhesion kinase: In command and control of cell motility. *Nat Rev Mol Cell Biol* 6(1):56–68.
47. Burridge K, Sastry SK, Sallee JL (2006) Regulation of cell adhesion by protein-tyrosine phosphatases. I. Cell-matrix adhesion. *J Biol Chem* 281(23):15593–15596.
48. Golji J, Wendorff T, Mofrad MR (2012) Phosphorylation primes vinculin for activation. *Biophys J* 102(9):2022–2030.
49. Bregeon J, Loirand G, Pacaud P, Rolli-Derkinderen M (2009) Angiotensin II induces RhoA activation through SHP2-dependent dephosphorylation of the RhoGAP p190A in vascular smooth muscle cells. *Am J Physiol Cell Physiol* 297(5):C1062–C1070.
50. Kontaridis MI, et al. (2004) SHP-2 positively regulates myogenesis by coupling to the Rho GTPase signaling pathway. *Mol Cell Biol* 24(12):5340–5352.
51. Lacalle RA, et al. (2002) Specific SHP-2 partitioning in raft domains triggers integrin-mediated signaling via Rho activation. *J Cell Biol* 157(2):277–289.
52. Schoenwaelder SM, et al. (2000) The protein tyrosine phosphatase Shp-2 regulates RhoA activity. *Curr Biol* 10(23):1523–1526.
53. Kodama A, et al. (2000) Involvement of an SHP-2-Rho small G protein pathway in hepatocyte growth factor/scatter factor-induced cell scattering. *Mol Biol Cell* 11(8):2565–2575.
54. Zhang SQ, et al. (2004) Shp2 regulates SRC family kinase activity and Ras/Erk activation by controlling Csk recruitment. *Mol Cell* 13(3):341–355.
55. Chuang HH, et al. (2012) ROCKII Ser1366 phosphorylation reflects the activation status. *Biochem J* 443(1):145–151.
56. von Wichert G, Haimovich B, Feng GS, Sheetz MP (2003) Force-dependent integrin-cytoskeleton linkage formation requires downregulation of focal complex dynamics by Shp2. *EMBO J* 22(19):5023–5035.
57. Wang YL, Pelham RJ, Jr. (1998) Preparation of a flexible, porous polyacrylamide substrate for mechanical studies of cultured cells. *Methods Enzymol* 298:489–496.
58. Hur SS, Zhao Y, Li YS, Botvinick E, Chien S (2009) Live cells exert 3-dimensional traction forces on their substrata. *Cell Mol Bioeng* 2(3):425–436.

Supporting Information

Lee et al. 10.1073/pnas.1222164110

SI Materials and Methods

Plasmids and Reagents. Expression constructs of wild-type and Y722F Rho-associated protein kinase II (ROCKII) were subcloned into pEGFP vector. The pRFP-vinculin expression vector was kindly provided by C. H. Lin (Institute of Microbiology and Immunology, National Yang-Ming University).

The production of the anti-pY722 ROCKII and anti-pS1366 antibodies have been described previously (1, 2). Anti-paxillin antibody from BD Biosciences, anti–β-actin, anti–β-tubulin antibodies and FITC-phalloidin from Sigma-Aldrich, anti-ROCKII, anti-RhoA, anti-FAK, anti-Shp2 (C-18 for Western blotting; B-1 for immunofluorescence staining) antibodies from Santa Cruz Biotechnology.

Cell Culture. $Shp2^{WT}$ and $Shp2^{Ex3-/-}$ mouse embryonic fibroblasts (MEFs) were kindly provided by Gen-Sheng Feng (3). Cells were maintained in Dulbecco's modified Eagle's medium (DMEM) supplemented with 10% (vol/vol) fetal bovine serum (FBS) in a humidified atmosphere of 5% CO_2/95% air at 37°C. For transient transfection experiments, cells were transfected by Micro-Porator MP-100 (Digital Bio Technology). NIH3T3 stable lines expressing wild type and Y722F myc-ROCKII have been described previously (1, 2).

Preparation of Polyacrylamide Gels. Elastic polyacrylamide (PAA) gels with Young's elastic modulus E of 2.5, 9.0, and 21.5 kPa were prepared based on the method developed by Wang and colleagues (4). The final concentrations of acrylamide/Bis-acrylamide were 5%/0.1% for 2.5 kPa gel, 10%/0.1% for 9.0 kPa gel, and 10%/0.2% (vol/vol) for 21.5 kPa gel. Gels were typically 30–40 μm thick. For cell adhesion, the bovine fibronectin (FN, 20 μg/mL; Sigma-Aldrich) was covalently cross-linked with PAA surface with the bifunctoinal cross-linker N-sulfosuccinimidyl-6-[4′-azido-2′-nitrophenylamino] hexanoate (sulfo-SANPAH, ProteoChem). For cellular traction force analysis, 0.04% (or 9.1×10^{10} per milliliter) of 0.2-μm diameter red fluorescent (580/605) polystyrene beads (Invitrogen), were added to the PAA solution before polymerization. The distance between beads was approximately 2.2 μm. The mechanical properties of the PAA gels were confirmed as reported elsewhere (5).

Cellular Traction Force Analysis. Cells were allowed to attach onto the FN-conjugated substrate overnight in cell culture media. Cell outlines were determined from differential interference contrast microscopy (DIC) images for cell area and cell shape analysis. The substrate deformation field was obtained from the lateral displacements of fluorescent beads embedded in the gel. Lateral bead displacements were determined by dividing each force-loaded image and the corresponding null-force image in interrogation windows, similar to our previous study (6). We then calculated the correlation function between pairs of boxes and found the displacement that maximizes the correlation. The procedure was performed using programs written in Matlab (MathWorks). The region of forces is determined to include the thin lamellipodia visible under DIC with 60× NA. The window separation was 32 × 32 pixels in the x and y directions leading to a spatial resolution of 3.4 μm. The lateral traction stresses exerted by the cells were determined the measured substrate deformation after solving the equation of static equilibrium for an elastic substrate, as described previously (5). This problem was solved with the finite element method using Abaqus (Dassault Systèmes). The traction stresses in the xy direction are showed by the arrows in traction stress vector plot (T_{xy}). The arrowheads indicate the stress direction, and both the width and length of the arrow stem indicate the stress magnitude (Fig 3*A*, *Top* row). The high NA (60×) used in our DIC microscopy includes the thin ruffles of the lamellipodia, which may not be seen with a lower NA. Because of the inclusion of the thin lamellipodia, the traction stress maximum is observed somewhat inside of the cell edges (Fig. 3*A*, *Middle* row).

The Net contractile moment (M) was calculated from the measured traction stresses by summing the diagonal components of the shear moment matrix in its principal form (M^{rot}). M = trace (M^{rot}) = $M_{xx}{}^{\mathrm{rot}} + M_{yy}{}^{\mathrm{rot}}$; where $M_{xx}{}^{\mathrm{rot}}$ and $M_{yy}{}^{\mathrm{rot}}$ represent the total contribution of cell-substrate contraction in the x and y direction, respectively (7, 8). The intracellular tension was determined similarly to Hur et al (9). We divided each cell in two different domains along intracellular sections of length $L_{1\text{-}2}$ (Fig. S1) and applied Newton's first law to each of the two domains to determine the average tension (force per unit section length) between them from the following equations

$$\int_{\text{domain 1}} \boldsymbol{\sigma}\, dS + \mathbf{F}_{1-2} = 0, \quad \text{and} \quad \int_{\text{domain 2}} \boldsymbol{\sigma}\, dS + \mathbf{F}_{2-1} = 0, \qquad \textbf{[S1]}$$

where $F_{1\text{-}2} = F_{2\text{-}1}$ is the total force supported by the cytoskeleton at the given intracellular section, and $T_{1\text{-}2} = T_{2\text{-}1} = F_{1\text{-}2} / L_{1\text{-}2} = F_{2\text{-}1}/L_{1\text{-}2}$ is the intracellular tension acting on the cytoskeleton (Fig. S1*A*). These equations state that the sum of the traction stresses over the area under each domain is balanced by the sum of the tension along the intracellular section. Because the intracellular tension is approximately perpendicular to the section's direction (9), the intracellular tensions along the major (long) and minor (short) axes of the cell are, T_S and major T_L, point in the direction of the short and long axes respectively (Fig. S1*B*). Fig. S1*C* shows maps of T_S and T_L for cells representative of each experimental condition in our study. In agreement with Hur et al. (9), both T_S and T_L increase with the distance to the cell boundary.

Immunofluorescence Staining. Cells were fixed with 3% (wt/vol) paraformaldehyde in PBS for 30 min, followed by permeabilization with 0.3% Triton X-100/Tris-buffered saline (TBS) for 5 min. After blocking with 5% (vol/vol) normal goat serum for 30 min, they were incubated overnight at 4°C with antibodies against paxillin (1:200) or phospho-Y722 ROCKII (1:100), then for 1 h with FITC or TRITC-conjugated secondary antibodies, FITC-phalloidin, and Hoechst, washed, mounted, and examined on a fluorescence microscope (AX70; Olympus) with a 100× oil lens. Images were captured with a digital camera and arranged using Photoshop software (Adobe).

Image Analysis. For analysis of focal adhesion (FA) characteristics, the images of immunofluorescent staining with anti-paxillin antibody or RFP-vinculin expressing cells were segmented and analyzed using ImageJ software. Areas of individual FAs and number of FAs per cell were determined. Segmentation and orientation analysis of cell stress fibers indicated by FITC-phalloidin staining was performed using an automated image analysis algorithm written in Matlab. The orientations of stress fibers were presented with different colors and summarized in a circular plot. Cell area, cell aspect ratio (the ratio of between the length of major and minor axes), and

cell shape factor (the ratio of cell perimeter to the perimeter of a circle with the same area) were measured by drawing the cell boundary and computing using Matlab-coded programs.

Isolation of FAs. The FAs were isolated as described by Kuo (10). Briefly, cells plated on a 100-mm dish coated with 10 μg/mL FN were washed with PBS and then hypotonically shocked with 5 mL of 2.5 mM triethanolamine in water at pH 7.0 for 2 min. Cell bodies were removed by pulsed hydrodynamic force with PBS containing 1 mM of PMSF, 5 mM of sodium fluoride (NaF), and 0.2 mM Na_3VO_4 using Waterpik (setting "3.5," Interplak dental water jet WJ6RW, Conair). The FAs remaining on the dish were collected by scraping with a rubber policeman with 2× Laemmli buffer for Western blot analysis.

1. Chuang HH, et al. (2012) ROCKII Ser1366 phosphorylation reflects the activation status. *Biochem J* 443(1):145–151.
2. Lee HH, Chang ZF (2008) Regulation of RhoA-dependent ROCKII activation by Shp2. *J Cell Biol* 181(6):999–1012.
3. Yu DH, Qu CK, Henegariu O, Lu X, Feng GS (1998) Protein-tyrosine phosphatase Shp-2 regulates cell spreading, migration, and focal adhesion. *J Biol Chem* 273(33): 21125–21131.
4. Wang YL, Pelham RJ, Jr. (1998) Preparation of a flexible, porous polyacrylamide substrate for mechanical studies of cultured cells. *Methods Enzymol* 298:489–496.
5. Hur SS, Zhao Y, Li YS, Botvinick E, Chien S (2009) Live cells exert 3-dimensional traction forces on their substrata. *Cell Mol Bioeng* 2(3):425–436.
6. Del Alamo JC, et al. (2007) Spatio-temporal analysis of eukaryotic cell motility by improved force cytometry. *Proc Natl Acad Sci USA* 104(33):13343–13348.
7. Butler JP, Tolić-Nµrrelykke IM, Fabry B, Fredberg JJ (2002) Traction fields, moments, and strain energy that cells exert on their surroundings. *Am J Physiol Cell Physiol* 282(3):C595–C605.
8. Prager-Khoutorsky M, et al. (2011) Fibroblast polarization is a matrix-rigidity-dependent process controlled by focal adhesion mechanosensing. *Nat Cell Biol* 13(12): 1457–1465.
9. Hur SS, et al. (2012) Roles of cell confluency and fluid shear in 3-dimensional intracellular forces in endothelial cells. *Proc Natl Acad Sci USA* 109(28):11110–11115.
10. Kuo JC, Han X, Hsiao CT, Yates JR, 3rd, Waterman CM (2011) Analysis of the myosin-II-responsive focal adhesion proteome reveals a role for β-Pix in negative regulation of focal adhesion maturation. *Nat Cell Biol* 13(4):383–393.

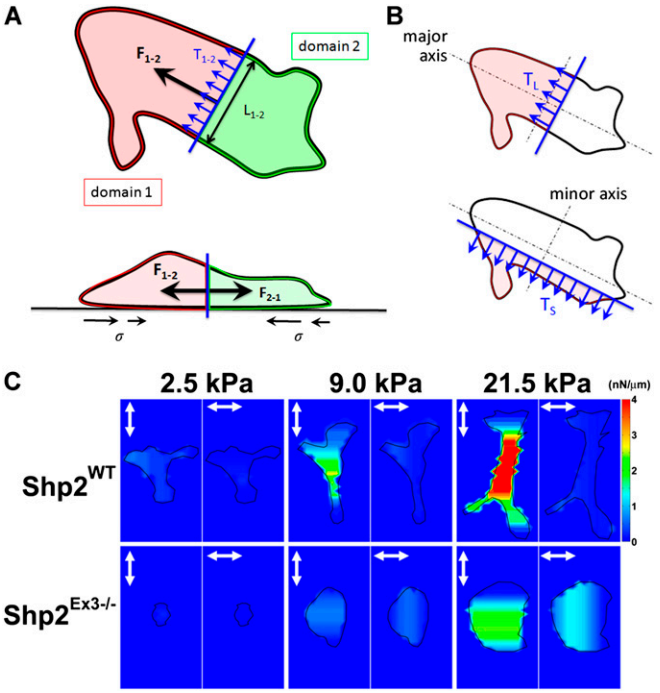

Fig. S1. Measurement of intracellular tension. Tension (T) is defined as force per unit length. (*A*) An adherent cell with traction stress on substrate (σ) is divided in two different domains. $T_{1\text{-}2}$ is the tension acting on domain 1 due to domain 2; $T_{2\text{-}1}$ is the tension acting on domain 2 due to domain 1; and $L_{1\text{-}2}$ is the length of the intracellular section that separates the two domains. (*B*) The intracellular tensions along the major (long) and minor (short) axes of the cell, T_S and major T_L, point in the direction of the short and long axes, respectively. (*C*) Maps of T_S and T_L for $Shp2^{WT}$ and $Shp2^{Ex3-/-}$ cells representative of each experimental condition in our study.

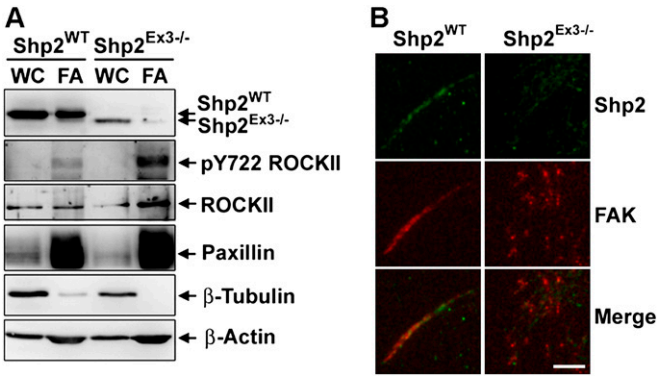

Fig. S2. Shp2 is recruited to focal adhesions. Shp2^{WT} and Shp2$^{Ex3-/-}$ MEFs were plated on FN-coated glass coverslips for 2 h for isolation of FAs as described in *Materials and Methods*. (*A*) Whole cell lysate (WC; from 2 x 10^4 cells) and isolated FA fraction (FA; from 2 x 10^6 cells) were subjected to SDS/PAGE and Western analysis with antibodies to the indicated proteins. Level of ROCKII Y722 phosphorylation in FA fraction was normalized to the corresponding ROCKII protein level in the same membrane blot, and the result showed 2.5-fold higher ROCKII Y722 phosphorylation in Shp2$^{Ex3-/-}$ cells than in Shp2^{WT} cells. (*B*) Isolated FAs were fixed and stained with anti-Shp2 (green) and anti-FAK (red) antibodies. (Scale bar, 5 μm.)

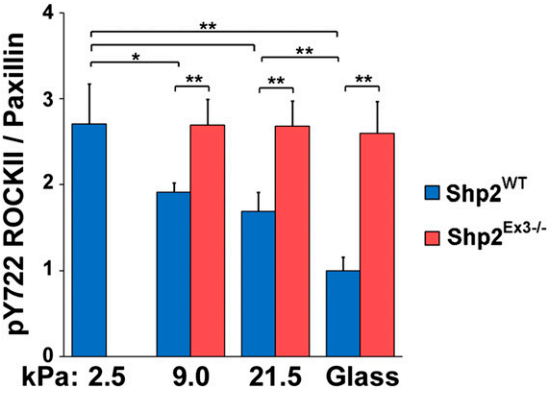

Fig. S3. Shp2 is essential for ROCKII Y722 dephosphorylation at FA region in response to matrix rigidity. Shp2^{WT} and Shp2$^{Ex3-/-}$ MEFs were plated on FN-conjugated gel with different rigidity or glass coverslips for 4 h as indicated. Cells were fixed and stained with anti-pY722 ROCKII and anti-paxillin antibodies. The ratio of the intensities of pY722 ROCKII versus paxillin intensities in the regions of FAs of each cell was measured and normalized with Shp2^{WT} cells seeded on glass coverslips. Data are mean ± SD. *P < 0.005, **P < 0.0005 (n = 10).

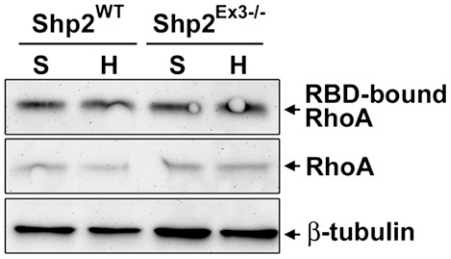

Fig. S4. RhoA activity in Shp2^{WT} and Shp2$^{Ex3-/-}$ MEFs. Shp2^{WT} and Shp2$^{Ex-/-}$ MEFs were plated on FN-conjugated soft (S; 2.5 kPa) and hard (H; 21.5 kPa) gels for 4 h. Cells were harvested for RhoA activity assay by GST-RBD pull-down assay. Levels of total RhoA and RBD-bound RhoA (active form) were determined by Western blotting with anti-RhoA antibody.

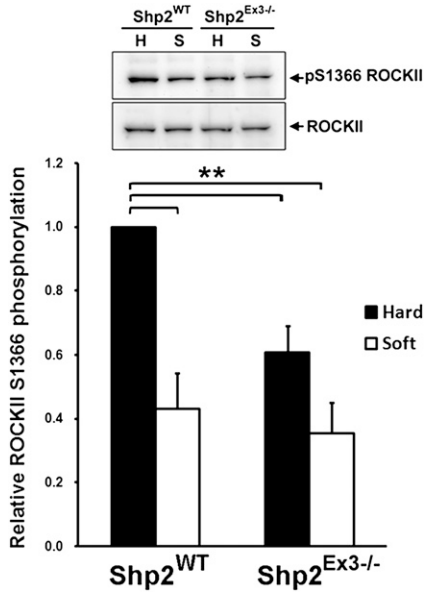

Fig. S5. Shp2 is required for the stiffness-dependent ROCKII activation. $Shp2^{WT}$ and $Shp2^{Ex3-/-}$ MEFs were plated on FN-conjugated soft (S; 2.5 kPa) and hard (H; 21.5 kPa) gels for 4 h. Cells were harvested for Western blotting with antibodies as indicated. One representative result is shown (*Upper*) and the quantification of relative ROCKII S1366 phosphorylation from three independent experiments is shown (*Lower*).

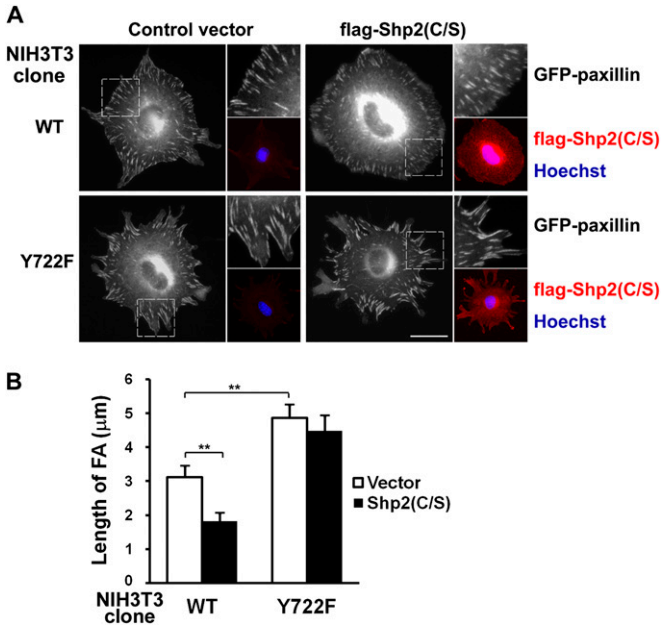

Fig. S6. Spatial variation in ROCK phosphorylation regulated by Shp2 during FA maturation. (*A*) NIH3T3 WT and Y722F clones were cotransfected with pEGFP-paxillin and a control or flag-Shp2(C/S) vector (DNA ratio 1:3) and plated on FN for 1 h. Cells were fixed and stained with anti-flag antibody (red) and Hoechst (blue). (*B*) Average length of FA of six different cells was measured and shown below.